Bioresource Technology 363 (2022) 127990

Contents lists available at ScienceDirect

Bioresource Technology

journal homepage: www.elsevier.com/locate/biortech

Continuous treatment of diethyl hexyl and dibutyl phthalates by fixed-bed reactor: Comparison of two esterase bionanocomposites

Esin Balci [a,b], Emilio Rosales [a], Marta Pazos [a], Aysun Sofuoglu [c], Maria Angeles Sanroman [a,*]

[a] CINTECX, Universidade de Vigo, Grupo de Bioingeniería y Procesos Sostenibles, Departamento de Ingeniería Química, Campus Lagoas-Marcosende, 36310 Vigo, Spain
[b] Izmir Institute of Technology, Faculty of Engineering, Department of Environmental Engineering, 35430 Urla/İzmir, Turkey
[c] Izmir Institute of Technology, Faculty of Engineering, Department of Chemical Engineering, 35430 Urla/İzmir, Turkey

HIGHLIGHTS

- Effective esterase immobilisation in halloysite alginate and chitosan nanocomposites.
- Immobilisation increased the stability of the enzyme along the time and reusability.
- Chitosan bionanocomposite achieved complete removal of DEHP and DBP.
- Feasible continuous treatment system developed for plastifiers treatment.

GRAPHICAL ABSTRACT

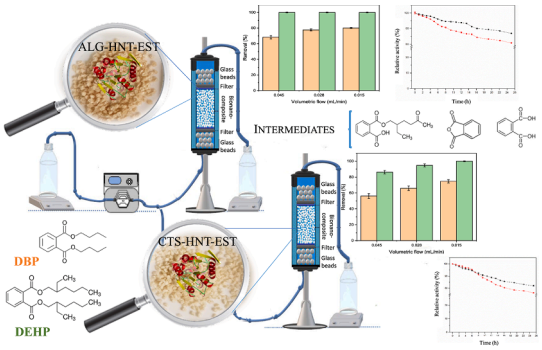

ARTICLE INFO

Keywords:
Halloysite
Bacillus subtilis
Enzymatic degradation
Phthalic acid esters
Immobilization

ABSTRACT

The removal of Diethyl hexyl phthalate (DEHP) and Dibutyl phthalate (DBP) is of great importance due to their potential adverse effects on the environment and human health. In this study, two bionanocomposites prepared by immobilization of *Bacillus subtilis* esterase by crosslinking to halloysite and supported in chitosan and alginate beads were studied and proposed as a green approach. The esterase immobilization was confirmed by physical–chemical characterization. Bionanocomposite using chitosan showed the best degradation levels in batch tests attaining complete degradation of DBP and around 90% of DEHP. To determine the operational stability and efficiency of the system, two fixed bed reactors filled with both bionanocomposites were carried out operating in continuous mode. Chitosan based bionanocomposite showed the best performance being able to completely remove DBP and more than 85% of DEHP at the different flowrates. These results proved the potential of these synthesized bionanocomposites to effectively remove Phthalic Acid Esters.

1. Introduction

Phthalic acid esters (PAEs) are one of the widely used synthetic chemicals in the plastic industry to supply the needs of modern society. Increasing demand for plastics has led to a significant increase in the global production of PAEs around the world. Today, PAEs have an

* Corresponding author.
E-mail address: sanroman@uvigo.es (M.A. Sanroman).

https://doi.org/10.1016/j.biortech.2022.127990
Received 3 August 2022; Received in revised form 13 September 2022; Accepted 14 September 2022
Available online 18 September 2022

annual production volume of over 8 million metric tons in the world (Weizhen et al., 2020). Owing to the fact that they do not have any covalent bond to the plastic matrix, they can be released into the environment during their manufacturing, use, and disposal. Once released, they reach almost all environmental media through geochemical processes, subsequently degrade very slowly under natural conditions, and lastly accumulate in the air, surface water, wastewater, sediment, soil, sewage sludge, and biota over time (Clark et al., 2003; Das et al., 2014). Dibutyl phthalate (DBP) and Diethyl hexyl phthalate (DEHP) are among the most abundant PAEs detected in the environment (Gao et al., 2020). They exhibit toxic, mutagenic, and carcinogenic properties even at low concentrations. Due to their high production volume, widespread distribution, and possible toxic effects, DBP and DEHP have been declared environmental priority pollutants by the United States Environmental Protection Agency (USEPA) and the European Union (EU). Besides, some nations in the EU and the United States of America have limited or prohibited their production and use. Therefore, the efficient removal of DBP and DEHP in the contaminated environment is of great importance. Various methods such as biodegradation and physical–chemical methods (photolysis, chemical hydrolysis, and oxidation) have been used to degrade DBP and DEHP in the environment. The biodegradation process has a major role in the removal of these pollutants. This is because it is a faster process than photolysis and hydrolysis, and results in innocuous end products. Biodegradation studies on PAEs comprise not only using bacterial strains but also using enzymes from these bacterial strains. Earlier reports also revealed that esterase is a major enzyme that acts on the ester bonds in the structure of PAEs. The esterase from *Bacillus* sp. (Niazi et al., 2001) and the esterase from *Bacillus* sp. K91 (Ding et al., 2015) were reported to be highly effective to degrade PAEs. Saito et al. (2010) underlined that pancreatic cholesterol esterase enzymes (50 U) completely degraded DBP and DEHP (5 μmol) within 15 min. Sun et al. (2022) reported that carboxyl esterase (0.1 U) was able to degrade more than 90% of DBP and DEHP (1 mg/L) in an aqueous solution within 288 h. The esterase appeared capable of degrading PAEs to their corresponding monoester and phthalic acid (PA) (Ding et al. 2015; Saito et al., 2010). Although there is information in the literature on the degradation of PAEs in the presence of the esterase enzyme obtained from various sources, no study was found on the use of the enzyme obtained from *Bacillus subtilis* in the degradation studies of PAEs.

Immobilization on a support material increases the stability and half-life of the enzyme and improves the resistance of the enzyme to changing environmental conditions such as pH, and temperature (Handayani et al., 2012; Wei et al., 2022). Enzymes can be bound by a support material using various immobilization methods such as adsorption, crosslinking, encapsulation, and entrapment. Among these methods, crosslinking is a very useful and preferable immobilization method. This is because it has various advantages over the stability and retention rate of the enzyme on support. Furthermore, the leakage of enzyme on support is low level. In enzyme immobilization, different support materials such as chitosan (Dulazi and Liu, 2011; Olshansky et al., 2018), alginate (Ramsay et al., 2005), silica (Chen and Lin, 2007) as well as alumina are used. Support materials must be water-insoluble and must have thermal, mechanical, and chemical stability, as well as resistance to microbial attack. At the same time, these materials must be low cost and must have biodegradability to harmless products. Among many supports, chitosan (CTS) and alginate (ALG) are the materials of interest in enzyme immobilization due to their wide availability and having most of the above-mentioned properties (Choo et al., 2016; Hurmuzlu et al., 2021). Furthermore, the reactive amino and hydroxyl groups of CTS that are effective on enzyme binding reactions provide a higher protein loading and higher activity (Hung et al., 2003; Dulazi and Liu 2011). However, it needs to improve its mechanical properties before an immobilization study (Peng et al., 2015; Choo et al., 2016). As for ALG, its use can be limited in various applications due to its swelling and degradation behavior in the water (Bhagyaraj and Krupa, 2020). To be used in many applications, it is necessary to minimize its swelling and improve its mechanical properties, that is, to extend its service life (Bhagyaraj and Krupa, 2020). It is possible to form composite beads with the addition of nano clay, carbon nanotubes (CNTs), and titanium dioxide to reinforce the mechanical properties of CTS and ALG. Among these materials, CNTs exhibit the potential to enhance the mechanical properties of support material. However, the synthesis process of CNTs is complicated and costly. Halloysite nanotube (HNT) with the formula of $Al_2Si_2O_5(OH)_4{\cdot}2H_2O$ is a natural aluminosilicate clay mineral with a large surface area and it is also cheap and easy to find. It has a tubular structure with abundant hydroxyl groups. All these properties of HNT support various modifications for different purposes. Due to the fact that HNT has excellent mechanical properties and thermal stability, it can reinforce the mechanical strength of CTS and ALG. There are only a few studies on forming of CTS with HNT (CTS-HNT) and ALG with HNT (ALG-HNT) beads in the literature. However, there are no studies about the esterase immobilization on CTS-HNT and ALG-HNT beads and their capability for the degradation of PAEs.

In this study, the main focus is the continuous degradation of DBP and DEHP by two bionanocomposites based on CTS-HNT and ALG-HNT beads. For this purpose, the amount of esterase immobilized on both bionanocomposites was analysed, the enzyme immobilization efficiency and stability was compared and the feasibility of the systems was tested by DBP and DEHP degradation in fixed-bed reactors operating in continuous mode.

2. Materials and methods

2.1. Materials

Pure HNT powder was provided by Esan, Eczacibasi Industrial Raw Materials Company (Istanbul, Turkey). Chitosan from crab shells, Bovine Serum Albumin (BSA), and Glutaraldehyde (GTA) were supplied from Sigma-Aldrich (USA). Sodium alginate was purchased from Quimipur, S.L.U. All other chemicals were of laboratory reagent grade and used without further purification. Esterase from *Bacillus subtilis* was obtained from Sigma-Aldrich. Before the immobilization study, HNT and CTS were dried in a vacuum oven at 100 °C and 40 °C, respectively to eliminate their moisture content and to make them ready for use. The esterase was stored at −20 °C until its use.

2.2. Immobilization study

2.2.1. Preparation of chitosan-halloysite beads

CTS-HNT beads were prepared with minor modifications to the previous studies (Choo et al. 2016; Hurmuzlu et al., 2021). Briefly, the procedure is described as follows: Firstly, 2 g of CTS were dissolved in 100 mL of acetic acid solution (2.5%, v/v). The mixture was stirred magnetically for 24 h at room temperature. Then, 1 g of HNT was added to the CTS solution and mixed for 24 h. Following this, the solution was sonicated for 1 h at ambient temperature to obtain a homogenous dispersion of CTS-HNT. The resultant solution was pumped into 125 mL of deionized water containing 15 g NaOH and 25 mL of 95% ethanol through a needle (diameter 1.2 mm) at a flow rate of 1 mL/min under stirring. Thereafter, the CTS-HNT spheres were formed instantaneously and washed with deionized water until neutral pH was reached. Subsequently, the beads were kept at −20 °C in the fridge overnight and then dried using a freeze dryer (lyophilizer) under vacuum conditions for 24 h at −50 °C (Telstar Cryodos).

2.2.2. Preparation of alginate-halloysite beads

3 g of sodium alginate were dissolved in 100 mL at 25 °C by mechanically stirring. 0.5 g of HNT was added to the sodium alginate solution. The solution was mixed until HNT was dispersed in an alginate solution at 300 rpm. After that, it was placed in an ultrasonicator for 1 h at room temperature. The obtained solution was dropped at a flow rate of 1 mL/min into calcium chloride solution (1 M) through a syringe

needle with a diameter of 1.2 mm under continuous stirring. The calcium chloride solution was kept at 4 °C before its use. The formed beads were taken from the solution and then washed with deionized water several times until the pH of the beads became neutral. Lastly, ALG-HNT beads were stored at −20 °C and then dried using a freeze dryer under vacuum conditions for 24 h at −108 °C. The dried CTS-HNT and ALG-HNT beads were stored until further use.

2.2.3. Immobilization of esterase on chitosan-halloysite and alginate-halloysite beads

In this study, GTA was used as crosslinking agent to immobilize the esterase enzyme on the beads. In previous studies, the amount of GTA in the solution required for the enzyme immobilization on beads has been used in the range of 0.072 mL (0.15%) and 0.36 mL (0.75%) and the optimal amount of GTA was determined to be 0.072 mL in the solution for 0.4 g of beads (Mondal et al., 2015). To prepare the crosslinked beads with GTA, 0.15% GTA solution (v/v) was added to 0.4 g of each bead. The solution with beads was mixed for 4 h at 25 °C and 150 rpm in an incubator shaker. To remove the non-crosslinked agent with beads, the beads were rinsed with deionized water three times. Thereafter, 1 mL of the enzyme (2 mg/mL) was added to the crosslinked beads and mixed on a test tube shaker at 25 °C, 80 rpm for 1 h. At the end of this period, the beads were filtered and washed with deionized water three times to remove the unbounded enzyme. After the immobilization process, the supernatant and washing solution was kept at 4 °C to determine the enzyme immobilization efficiency.

As result of these procedures, two different bionanocomposites were synthesized: CTS-HNT-EST and ALG-HNT-EST.

2.3. Protein determination

To determine the protein concentration of free and beads immobilized enzyme, the Bradford method was implemented. Firstly, a standard curve was created using Bio-Rad dye reagent and BSA as model protein. The absorbance of the solutions was measured using a UV–Visible spectrophotometer (Genesys-150) at the wavelength of 595 nm (Bradford, 1976). The protein concentration in the solutions was estimated using a calibration curve. Then, the amount of immobilized enzyme on the beads was calculated according to the mass balance. Immobilization efficiency (Imm.eff. (%)) and enzyme loading amount (Load. amount mg/mg) were calculated using the following equations (1–2);

$$\text{Imm. eff. } (\%) = \frac{\text{Initial protein amount} - (\text{protein amount in the supernatant and washing solution})}{\text{Initial protein amount}} x100 \quad (1)$$

$$\text{Load. amount } \left(\frac{\text{mg}}{\text{mg}}\right) = \frac{\text{Initial protein amount} - (\text{protein amount in the supernatant and washing solution})}{\text{mass of HNT}} \quad (2)$$

2.4. Enzyme activity assay

The enzyme activity of free and immobilized esterase was determined spectrophotometrically by hydrolysis of 4-nitrophenyl acetate (pNPC-2) according to Tekedar and Sanli-Mohamed (2011). For free esterase, the assay mixture (1 mL) consisted of 0.8 mL phosphate buffer (100 mM, pH = 7), 0.1 mL of 0.5 mM pNPC-2 dissolved in acetonitrile, and 0.1 mL of free enzyme solution (1 mg/mL). The activity of the immobilized enzyme was determined according to the activity measurement of the free enzyme. Instead of free enzyme solution, 0.1 mL of supernatant and/or washing solution was added to the assay mixture. Then, the assay mixture was incubated at optimum temperature for 5 min and initial rates were estimated by measuring the increase in absorbance at 400 nm as a function of time. The activity of the immobilized enzyme was determined depending on the calculated activity of the free enzyme. The enzyme activity (U/L) was calculated according to the following equation (3).

$$\text{Enzyme activity } (\text{U/L}) = \frac{(\text{Absorbance at 400 nm }) \ (\text{Vt}) \ (\text{DF})}{(\text{t}) \ (\text{h}) \ (\text{Ve}) \ (\text{d})} \quad (3)$$

Vt: total sample volume (mL), DF: dilution factor, t: reaction time (min), Ɛ: p-nitrophenol molar extinction coefficient at 400 nm (17,215 $M^{-1}{\cdot}cm^{-1}$), V_e: enzyme volume (mL), d: light path (1 cm).

Besides, after each day of degradation experiments, the activity of the immobilized enzyme was measured and then expressed as relative activity (He et al., 2015).

2.5. Material characterization

Before and after enzyme immobilization, HNT, CTS-HNT, and ALG-HNT were structurally characterized by Scanning Electron Microscopy (SEM), Transmission Electron Microscopy (TEM), Fourier Transform Infrared Spectroscopy (FT-IR). To investigate the thermal resistance of these materials, Thermogravimetric Analysis (TGA) was conducted. These analyses were done by the external services of CACTI (University of Vigo).

2.5.1. Scanning Electron Microscopy analysis

The microstructure of pure HNT, CTS-HNT, and ALG-HNT beads and the beads with esterase was examined using an FEI QUANTA 250 FEG Scanning Electron Microscopy (SEM) instrument equipped secondary detector. Before SEM analysis, the samples were dried and their surface was coated with gold in argon to eliminate the charging of the beam.

2.5.2. Transmission Electron Microscopy analysis

The morphological properties of HNT, CTS-HNT, and ALG-HNT beads were investigated using a MICRO JEOL JEM 1010 Transmission electron microscopy (TEM) with an accelerating voltage of 200 kV. Before TEM analysis, both HNT and the beads with HNT were dispersed in ethanol solution using an ultrasonic bath. Subsequently, a drop of each dispersion was deposited on a 400 mesh carbon-coated copper grid. The sample grids were kept at room temperature to evaporate ethanol.

2.5.3. Fourier-Transform Infrared Spectroscopy analysis

Before FTIR analysis, the samples were mixed with potassium bromide (KBr) and pelletized. FT-IR spectra of the HNT, CTS-HNT, ALG-HNT, CTS-HNT with esterase, and ALG-HNT with esterase were recorded on a JASCO FT-IR 4100 spectrometer (Jasco Inc., Easton, MD, USA) to examine functional groups. All spectra were scanned in the range of 4000–400 cm^{-1} at a resolution of 2 cm^{-1}.

2.5.4. Thermogravimetric analysis

The thermal behavior of CTS-HNT with esterase and ALG-HNT with esterase was investigated using a Seteram thermogravimetric analyzer a temperature range that started at the room temperature and ended at 800 °C at a heating rate of 10 °C/min under nitrogen atmosphere (20

mL/min).

2.6. Degradation assays

2.6.1. Assays with free esterase

For the experiment on DBP and DEHP (100 mg/L) degradation, a reaction mixture (1 mL) containing 0.1 mL of free esterase solution (1 mg/mL), 0.1 mL of DBP/DEHP (1000 mg/L) in DMSO, 0.1 mL of Tween 80 (1%, v/v) and 0.7 mL of phosphate buffer (0.5 mM, pH = 7) was prepared. Tween-80 was used as a solubility agent to increase the solubility of DBP and DEHP in the solution. Under optimum conditions, the samples containing the reaction mixture were incubated at certain time intervals for 1 h and subsequently were collected. All samples were filtrated with a 0.22 μm PTFE syringe filter to remove particulate material from the samples before HPLC analysis. Subsequently, 1 M HCl (10% v/v) was added to the samples to stop the enzymatic reaction and the samples were stored at 4 °C until the analysis.

2.6.2. Assays with bionanocomposites

Enzymatic experiments were conducted in two column systems filled with CTS-HNT-EST and ALG-HNT-EST. 0.4 g of beads containing esterase were placed in the column. Initially, the batch experiments were performed by filling the column with DBP or DEHP solution with an initial concentration of 100 mg/L.

For the continuous process, the systems were fed with the DBP solution with a concentration of 100 mg/L under different volumetric flows (0.015–0.045 mL/min). After DBP degradation experiments were completed using each bead with esterase, DEHP degradation experiments were performed under the same conditions. During continuous operation, samples were collected in the system to determine the enzyme and pollutants concentration. All samples were filtered through a 0.22 μm PTFE syringe filter to remove particulate material prior to High-Performance Liquid Chromatography (HPLC) analysis. To terminate the enzymatic reaction, 1 M HCl (10% v/v) was added to the samples, which were then stored at 4 °C in a fridge.

2.6.3. Analysis of phthalates and their metabolites

After degradation experiments, the quantification of DBP and DEHP was analyzed under a reversed-phase using an HPLC Agilent 1260 Infinity connected to a DAD equipped with a ZORBAX Eclipse XDB C-8 column (5 μm particle size, 150 mm × 4.6 mm i.d.). The mobile phase consisting of acetonitrile:water (60:40, v/v) was used at a flow rate of 1 mL/min for DBP analysis. As for DEHP analysis, the mobile phase composition (acetonitrile:water) in gradient elution was varied over time as follows: 0 to 3 min 80:20, 3 to 9 min 95:5, 9 to 12 min 100:0, 12 to 22 min 80:20 and the flow rate was set at 0.5 mL/min. For each injection, the volume taken from samples in DBP and DEHP analysis was 20 μL and 10 μL, respectively. The analysis was carried out together with a UV detector (224 nm) at room temperature. DBP and DEHP degradation metabolites were identified using a Bruker Elute LC system connected to a Trapped Ion-Mobility Spectrometry Time-of-Flight Mass Spectrometer (TIMS-TOF-MS) (Bruker Daltonics, Bremen Germany). Ionization was performed using electrospray (ES) source with a voltage of 3.5 kV applied to the needle and an endplate offset of 500 V. Using both positive and negative scan modes, ES spectral data was obtained. The data were obtained using Bruker Otof Control Software version 5.1 and processed with the Data analysis software version 5.1 from Bruker Daltonics.

3. Results and discussion

3.1. Assays with free esterase

3.1.1. Effect of the operational condition on the esterase activity

In this study, an esterase obtained from *Bacillus subtilis* was selected to evaluate its efficiency in the removal of PAEs. Although it is a mesophilic enzyme, the effect of temperature on the enzyme activity was measured in a wide temperature range from 20 °C to 70 °C and examined for a solution pH between 5 and 7.

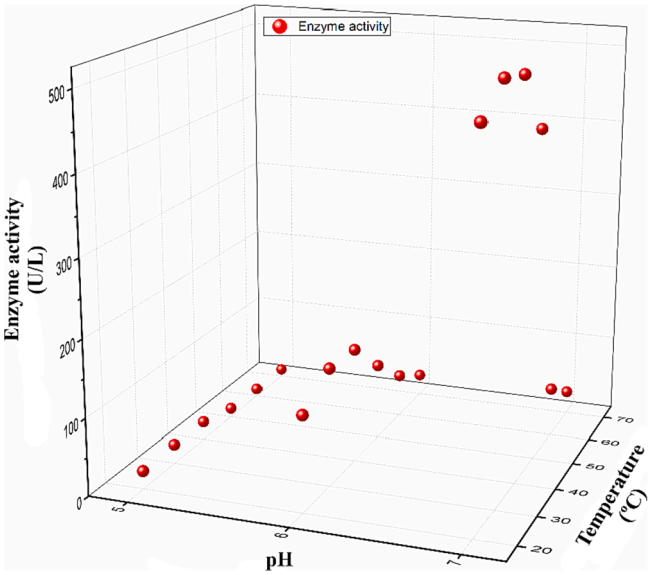

Fig. 1. Esterase activity under different conditions.

As shown in Fig. 1, the activity of the esterase increased with the temperature rising to 30 °C in the presence of pNPC-2 substrate. However, the increase above 40 °C caused a sharp decrease in the activity of the esterase. These results are in accordance with the reported in the literature where it is noted that temperatures above 30 °C are likely to cause a decrease in the activity of the enzyme (Fitter et al., 2001). Besides, the importance of pH on the enzyme activity was probed to be quite high at pH 7 compared to the more acidic investigated pH values. Therefore, the optimum temperature and pH for esterase were determined to be 30 °C and 7, respectively. Once the optimal operational conditions were evaluated the degradation capacity of the enzyme for two different PAEs (DEHP and DBP) was studied.

3.1.2. Degradation assays

Enzymatic degradation experiments of DBP and DEHP (100 mg/L) were performed using free esterase enzyme (1 mg/mL) under optimum

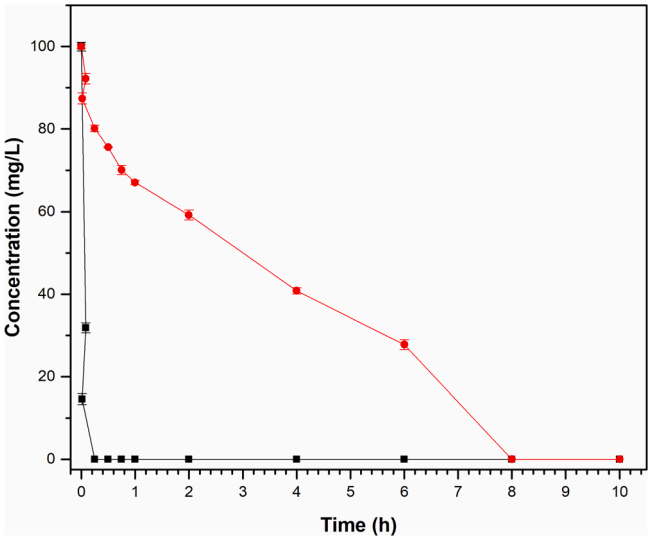

Fig. 2. Time-dependent DBP (■) and DEHP (●) concentration changes in the presence of free esterase (1 mg/mL).

conditions. Fig. 2 shows the change of DBP and DEHP concentration over time in presence of the esterase. While the esterase was able to completely degrade DBP for 15 min, it could not exhibit the same degradation ability on DEHP within the same time. At the end of 15 min, DEHP concentration was approximately 80.13 mg/L. It is apparent from Fig. 2 that the free esterase can degrade DEHP more slowly. It is known that PAEs with lower molecular weight such as DBP are more easily degraded compared to those with high molecular weight such as DEHP (Dulazi and Liu, 2011). Zhang et al. (2014) conducted a study on the degradation of different PAEs types using the esterase enzyme obtained from *Sulfobacillus acidophilus DSM10332*. They reported that six PAEs (Diethyl phthalate (DEP), Dipropyl phthalate (DPrP), DBP, Dipentyl phthalate (DPeP), Dihexyl phthalate (DHP), and Benzyl butyl phthalate (BBP)) were completely degraded to their monoesters within 24 h, but two PAEs, namely DEHP and Dicyclohexyl phthalate (DCHP), could not be degraded in the same period. Many studies have highlighted that the degradation rate of PAEs may decrease with the increase of the molecular weight (Ren et al., 2016). For this reason, the degradation of DEHP may take a longer time than that of DBP in this study. As can be seen from Fig. 2, DEHP was completely degraded within 8 h in the presence of the esterase.

3.2. Characterisation of bionanocomposites

The free enzyme proved to be a viable alternative for the treatment of PAEs. However, the enzyme's resistance to changing environmental conditions and allowing its use in a continuous treatment system needs to be developed. This purpose can be achieved by its immobilization in a suitable matrix. The immobilization of the enzyme in clay support such as HNT by crosslinking allows to achieve the anchoring of the enzyme, but for an application, in continuous treatment, the generation of a powder is discouraged by the operational problems generated in these treatment systems. Thus, the combination of the HNT with the immobilized enzyme generating both CTS and ALG based beads was carried out. The enzyme immobilization efficiency of the esterase in CTS-HNT-EST and ALG-HNT-EST was evaluated attaining 89.2% and 95.2% efficiency (Eq. (1)), respectively. Moreover, the loss rate of enzyme activity in the immobilized process on CTS-HNT and ALG-HNT is 17.83% and 18.66%, respectively. The prepared bionanocomposites (CTS-HNT and ALG-HNT beads) were characterized in order to determine their morphological and chemical properties.

The three-dimensional tubular structure of pure HNT and its surface was recognized in the SEM images (see supplementary material). The length of the HNT is not uniform and ranges from 0.4 to 1 μm. The diameter of HNT is more or less 30 nm and its outer surface is between 70 and 100 nm. Additionally, its average wall thickness is approximately 10 nm. SEM images of CTS-HNT and ALG-HNT beads (see supplementary material) before and after enzyme immobilization at different magnifications show that the beads containing HNT have a rough, dense, and compact structure. Similar observations have been reported in previous studies (Zhai et al., 2013; Hurmuzlu et al., 2021). Zhai et al. (2013) underlined that after modification of HNT with CTS, the surface of the CTS-HNT composite is rougher than that of pure HNT. The roughness of the surface increases the enzyme immobilization efficiency when creating a new surface area on material for enzymes (Zhai et al., 2013). HNT in the beads is not visible, however, it can be seen that HNT was covered by CTS and ALG, respectively. Esterase immobilized on CTS-HNT and ALG-HNT formed new regions by partially reducing the roughness on the surfaces of the beads. On the other hand, esterase immobilization changed the surface morphology of the beads. Consequently, this implies that enzyme immobilization has been successfully performed.

TEM images of the pure HNT revealed that the HNT has a hollow cylindrical structure with a transparent central area and two open ends (see supplementary material). Before and after enzyme immobilization, TEM images of CTS-HNT and ALG-HNT beads were taken and the tube structure of HNT is visible on both beads (see supplementary material).

After enzyme immobilization, the presence of esterase is observed in TEM images of CTS-HNT and ALG-HNT beads. There is a slight increase in the outer diameter of the nanotubes in the beads with esterase. Zhai et al. (2013) stated that the HNT with enzyme is rougher and thicker than pure HNT. This result shows that the enzyme is loaded on CTS-HNT and ALG-HNT beads.

The infrared spectrum of pure HNT shows the O—H stretching of water at 3696 cm^{-1}, and the OH deformation of water at 3625 cm^{-1}. The sharp peak at 1033 cm^{-1} originated from in-plane Si-O-Si stretching vibration (Luo et al., 2010). The peaks correspond to the deformation vibrations of inner surface hydroxyl groups at 910 cm^{-1} and 693 cm^{-1}. Besides, the peaks observed at 754 cm^{-1} and 540 cm^{-1} could be attributed to perpendicular stretching of Si-O and deformation of Al-O-Si, respectively (Luo et al., 2010). It can be observed that CTS-HNT samples (see supplementary material) exhibited some new peaks at 1639–1650 cm^{-1} (amide I) and 1529–1535 cm^{-1} (amide II) compared to pure HNT. The amide I (1630 cm^{-1}) and amide II (1535 cm^{-1}) bands are the two most prominent vibrational bands of the protein backbone (Jang et al., 2015). In addition, the spectra of CTS-HNT composite samples appear to contain characteristic peaks of both HNT and CTS. These results demonstrate that HNT has been successfully combined with CTS in this study. With the addition of GTA to CTS-HNT beads, three prominent peaks of GTA (1708, 1654, and 1562 cm^{-1}) are observed. After the immobilization of esterase, there is a small modification in the FT-IR spectrum of CTS-HNT-EST implying the immobilization of esterase.

The FT-IR spectrum of ALG (see supplementary material) contains a broad band centered at approximately 3250 cm^{-1} due to the stretching of hydroxyl groups. The band at 2900 cm^{-1} is assigned to $–CH_2$ groups. The two peaks at 1610 cm^{-1} and 1417 cm^{-1} arise due to the asymmetric and symmetric stretching modes of carboxylate salt groups (-COONa), respectively. The vibrations in the range of 1200 cm^{-1} and 1000 cm^{-1} come from the glycoside bonds in the polysaccharide (C—O—C stretching). The spectrum of EST crosslinked on ALG-HNT beads indicated the characteristic peaks of ALG, HNT, and EST. After the immobilization of enzymes, the intensity of the peak attributed to the asymmetric stretching of carboxylate salt groups decreased. This result implies the esterase has been successfully immobilized on the ALG-HNT beads.

TGA results were determined for studying the degradation trend of the prepared beads (see supplementary material). The decomposition of protein under air flow shows a maximum mass loss between 300 °C and 350 °C (Duce et al., 2017). In addition, a shoulder is observed at 245 °C due to the polypeptide chain thermal decomposition of esterase (Duce et al., 2013). At 450 °C and 650 °C, esterase undergoes the decomposition of aggregates as well as the carbonizing and ashing of the hard residues of the proteins (Duce et al., 2017).

Thermal degradation of CTS-HNT-EST and ALG-HNT-EST is observed in two stages. In the first stage, the thermal degradation of CTS-HNT-EST in the range of 25 °C and 100 °C is caused by the loss of the physically adsorbed water molecules (Lisuzzo et al., 2020). As for ALG-HNT-EST, the weight loss between 70 °C and 90 °C can be attributed to the evaporation of loosely bound moisture. In the second stage, while degradation of CTS-HNT-EST, vaporization and elimination of volatile compounds occurred between 170 °C and 500 °C (Hurmuzlu et al., 2021). The reduction of ALG-HNT-EST in the range of 190 °C-280 °C can be attributed to the evaporation of glycerol and the thermal degradation of the biopolymer (Bhagyaraj and Krupa, 2020). As a result, the bionanocomposites obtained by immobilization of esterase on CTS-HNT and ALG-HNT beads significantly improved the thermal resistance of the enzyme.

3.3. Batch degradation assays with bionanocomposites

The use of enzymes on a large scale demands operational stability from the bionanocomposite as a key factor in the processes and also to

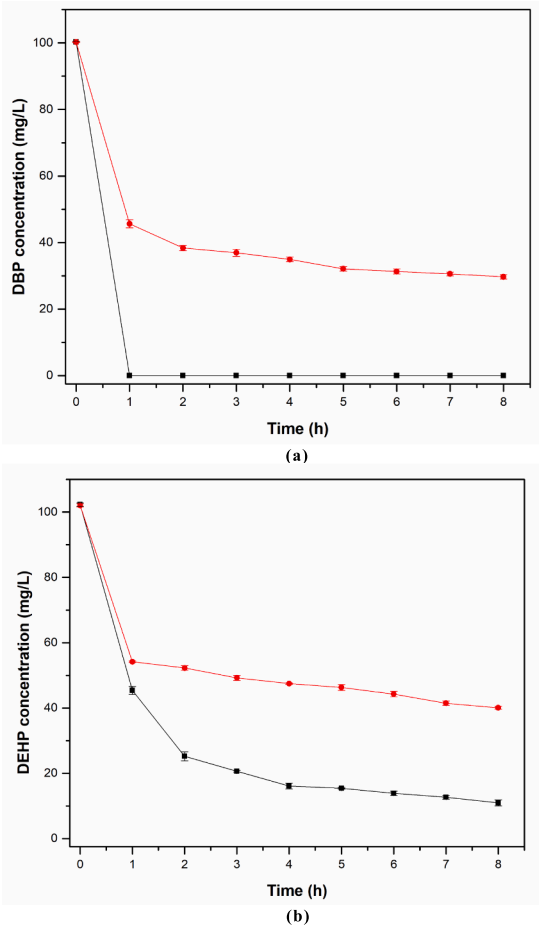

Fig. 3. Profile of concentrations of (a) DBP and (b) DEHP in their degradation by CTS-HNT-EST (■) and ALG-HNT-EST (●).

decrease operational costs.

Based on the promising previous results, the ability of the bionanocomposites for the degradation of DBP was ascertained in a batch system and the attained results are shown in Fig. 3. A significant difference is observed depending on the selected bionanocomposite. The structural differences between them suggest that the enzyme is more available when CTS-HNT-EST was used with complete removal of the pollutant in only 1 h. The process is slower in ALG-HNT-EST attaining less than 70% of removal after 4 h.

The good results achieved in the DBP degradation suggested that the system could be applied for the removal of a more complex compound such as DEHP and the study of the effect of the chain length in the biocomposites degradation of the pollutants was performed. According to the results, it can be assumed that a rapid degradation process occurs in the first hour, followed by a significant reduction in the degradation rate after the sixth hour. No complete degradation is achieved with any of the bionanocomposites meaning that the length of the pollutant chain affects the treatment process. They present a higher degradation ability for PAEs with lower molecular weights. This is in accordance with the reported in the literature by Dulazi and Liu (2011) who reported similar behavior for lipase immobilized in chitosan beads.

As conclusion from the batch assays, it can be suggested that there are two plausible mechanisms involved in the process: (i) direct degradation by the immobilized enzyme and (ii) the combination of adsorption and degradation in the process. For this reason, the possible generation of metabolites during the treatment process was ascertained confirming the degradation process is taking place.

The metabolites, generated during the degradation processes, were identified using LC-MS and the ratios of the compounds obtained by mass spectrometry were confirmed with the ratios of the same compounds in the literature (see supplementary material). DBP solution without enzyme was used as control sample in the analysis. Initially, DBP was identified and at the end of the degradation experiment in the presence of free esterase for 15 min. There was a signal showing the presence of phthalic anhydride ($C_8H_4O_3$), which is a product formed due to the dehydration of PA. According to the literature, it is known that the biodegradation mechanism of PAEs begins with the hydrolyzation of the ester bond in the presence of esterase. PAE is converted to its monoesters and then to PA and corresponding alcohol (Wang and Gu, 2006). Lastly, the mineralization mechanism ends with the decomposition of PA and CO_2 and/or CH_4 by microorganisms (Staples et al., 1997). Mono Butyl Phthalate (MBP), Dimethyl phthalate (DMP) and PA products have been also detected as intermediates in the actual degradation assays. Generally, Butyl methyl phthalate (BMP), MBP, DMP, and PA are detected as the potential metabolites of DBP that occur via transesterification or/and de-esterification reaction in the presence of methanol (Kim and Lee, 2005; Ahn et al., 2006; Kumar et al., 2017). Kim and Lee (2005) conducted a study on the enzymatic degradation of DBP. They reported that BMP was the major metabolite to appear in DBP degradation conducted using the esterase. Fang et al. (2017) focused on the degradation of DBP using a bacterium (*Enterobacter* sp. T5) which was isolated from municipal solid waste. They underlined MBP and PA as major metabolites of DBP in the study. In a study by Fang et al. (2017), 1,2 Benzenedicarboxylic acid, Butyl methyl ester, DMP, and PA were among the metabolites detected as an indicator of DBP degradation. Wang et al. (2017) conducted a study on DBP degradation using a bacterial consortium (LV-1). They identified three major metabolites (MBP, Monoethyl phthalate (MEP), and PA) at the end of DBP degradation experiments. In another study on DBP degradation, DBP was degraded to PA after the formation of MBP, MEP, and Monomethyl phthalate (MMP) (Ahuactzin-Perez et al., 2018). However, most of the above-mentioned metabolites may not have appeared in this study due to the use of DMSO as an organic solvent to dissolve PAEs. This is because in the absence of methanol, PAEs undergo transformation only via the sequential hydrolysis of ester and the esterification of the carboxylic acid in the monoester forms does not occur (Okamoto et al., 2011). It is apparent from LC chromatograms that DBP was degraded to phthalic anhydride by esterase immobilized on CTS-HNT and ALG-HNT. Phthalic anhydride that appeared in the presence of free esterase during DBP degradation was also found in the presence of the esterase immobilized on CTS-HNT and ALG-HNT beads. These results demonstrate that both free esterase and the immobilized esterase degraded DBP to Phthalic anhydride and imply that after immobilization, the esterase has the potential to be used as an effective degrader in long cycles without losing all of its characteristics.

Similarly, DEHP as well as three degradation products, 1,3-isobenzofurandione (IBF), Phthalic anhydride and mono-2-ethylhexyl phthalate (MEHP), were identified when metabolites related to DEHP degradation were investigated. During this degradation process, DEHP was converted to IBF by diester hydrolysis. The formation of MEHP and PA was also reported as the result of enzymatic or bacterial degradation of DEHP (Saito et al. 2010). Besides, Feng et al. (2002) conducted a study on DEHP biodegradation using a bacterium (*Pseudomonas fluorescens* FS1) isolated from the activated sludge at a petrochemical factory. Mono (2-Ethylhexyl) phthalate, benzene dicarboxylic acid, benzoic acid, and phenol were identified as the major metabolites of DEHP in the study. Yang et al. (2018) studied DEHP degradation using *Rhodococcus ruber* YC-YT1 and reported that DEHP was hydrolyzed to PA through the formation of MEHP. Subsequently, the bacterium converted PA to benzoic acid for cell proliferation in the study. DEHP metabolites which were defined based on the information compiled from the literature were also found in this study. The signal at 11.2 min observed in the chromatogram belongs to the polymer. When the chromatograms related to DBP and DEHP degradation are examined, the retention time

of PA is different for each chromatogram. The reason for this is the use of different methods in the LC-MS analysis of the two PAEs. While the immobilized esterase on CTS-HNT and ALG-HNT was able to degrade DEHP to Phthalic anhydride, the free esterase enzyme was incubated in DEHP solution for 8 h, and it degraded DEHP to MEHP. It may be related to the steric hindrance of MEHP which has carboxyl groups inhibiting free enzymes to bind the substrate (Liang et al., 2008). That is, the side chain of MEHP hampers the binding site of hydrolytic enzymes (Liang et al., 2008; Singh et al., 2017). Therefore, the hydrolysis of MEHP is hindered and thus the hydrolysis reaction is inhibited. There are some studies where the steric hindrance near the ester bonds inhibits the rate of hydrolysis. Singh et al. (2017) studied DMP and DEHP degradation using *Arthrobacter* sp. C21. They reported that the degradation efficiency of DMP (99.5%) was higher than that of DEHP (51.4%) and underlined that this is due to the steric hindrance caused by the side ester chain of DEHP.

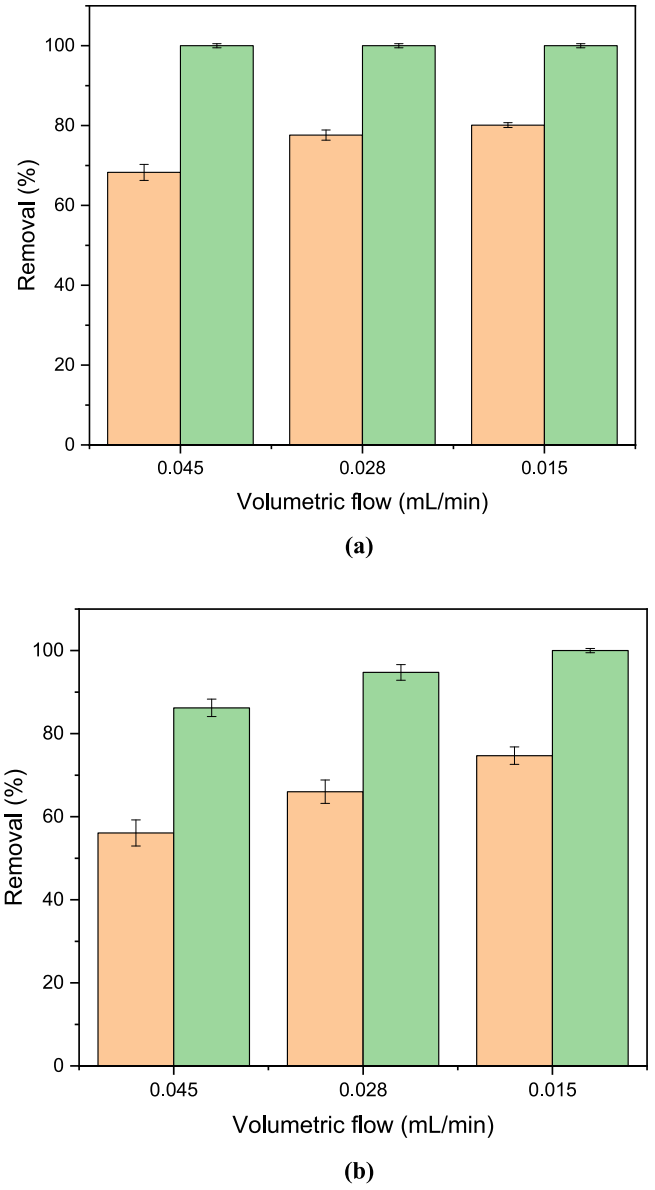

Fig. 4. Pollutants removal of (a) DBP and (b) DEHP operating in continuous under different volumetric flows in the presence of the CTS-HNT-EST (green) and ALG-HNT-EST (brown). (For interpretation of the references to colour in this figure legend, the reader is referred to the web version of this article.)

3.4. Continuous degradation

Once the efficiency of the degradation of the pollutants and their mineralization has been proved, the proposed treatments have been evaluated in a continuous flow system for the removal of both pollutants (DBP and DEHP).

3.4.1. Dibutyl phthalate bionanocomposite degradation

Fig. 4a shows the stationary DBP concentrations attained in continuous degradation experiments in the presence of the CTS-HNT-EST and ALG-HNT-EST bionanocomposites at different volumetric flows.

Operating at a flow rate of 0.045 mL/min, it can be observed that the alginate bionanocomposite reduced DBP significantly until values close to 30 mg/L. However, the selection of chitosan bionanocomposite led to the complete removal of DBP. This fact can be due to differences in the enzyme activity. The chitosan bionanocomposite resulted in a lower loss of activity and, thus, higher degradation capability in comparison with the alginate composite (ALG-HNT-EST) which lost two-folds the relative activity. The reduction of the volumetric flow to 0.030 mL/min (led to an improvement in the efficiency of the removal with ALG-HNT-EST attaining a DBP concentration value of 21 mg/L and degradation level of around 80%. As can be expected according to the previous results, CTS-HNT-EST bionanocomposite was able to remove all the DBP. After the degradation tests were completed, it was observed that DBP was completely degraded in the presence of the CTS-HNT-EST

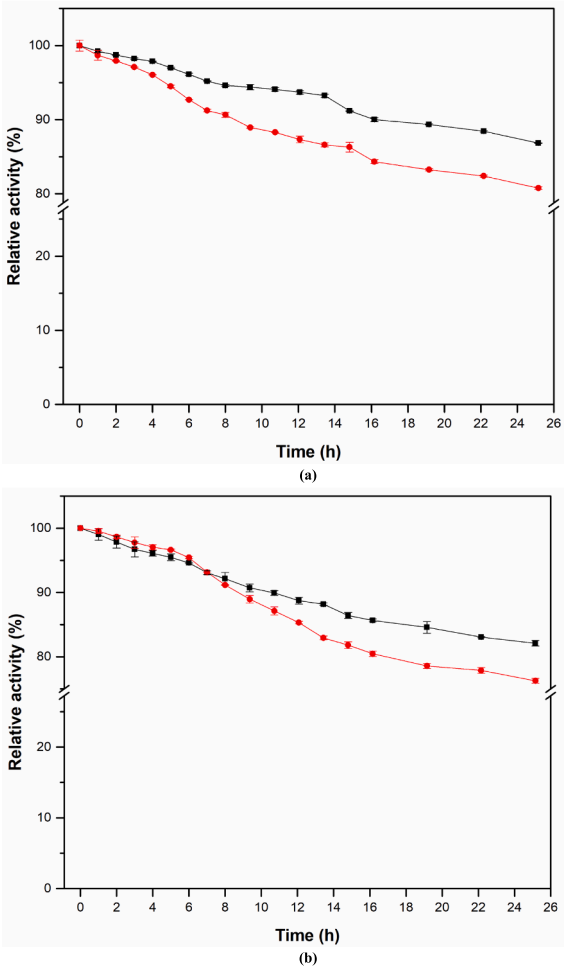

Fig. 5. (a) Relative activity of the esterase immobilized on CTS-HNT-EST (■) and ALG-HNT-EST (●) during the DBP degradation. (b) Relative activity of the esterase immobilized on CTS-HNT-EST (■) and ALG-HNT-EST (●) during the DEHP degradation.

bionanocomposite when the volumetric flow was still decreased (0.015 mL/min). However, no total degradation was detected for ALG-HNT-EST bionanocomposite with a concentration found to be 19.11 mg/L. This fact can be related to the enzymatic activity retained after the treatment. The degradation efficiency of DBP in presence of ALG-HNT-EST at a flow rate of 0.045, 0.028, and 0.015 mL/min was 70%, 80%, and 81%, respectively. Thus, reducing the volumetric flow prolonged the contact time of DBP with the bionanocomposites. This fact may be the reason for the increased degradation efficiency of DBP in column experiments.

Fig. 5a shows the relative activity of the esterase crosslinked on the bionanocomposites. In all the evaluated flows, ALG-HNT-EST bionanocomposite presented a higher decrease in the enzyme activity with values 5% lower than the detected within CTS-HNT-EST bionanocomposite. At the end of the experiments, ALG-HNT-EST retained 79% of its initial activity while CTS-HNT-EST retained over 85% of its initial activity indicating that they have good operational stability operating in a continuous way. The values are in good agreement with the reported by Tercan et al. (2021) in the esterase entrapment using chitosan/calcium/alginate-blended beads with more than 70% of the enzyme activity after three subsequent cycles. Yoo et al. (2020) also reported good operational stability (70%) by using crosslinked enzyme aggregate (CLEA) for twenty cycles. Accordingly, at the end of DBP degradation experiments, the enzyme mass (%) on CTS-HNT and ALG-HNT was found to be 86.48% and 80.2%, respectively.

3.4.2. *Diethyl hexyl phthalate bionanocomposite degradation*

The profiles of DEHP concentration during the treatment with the bionanocomposites at different flow rates in the presence of esterase immobilized on CTS-HNT-EST and ALG-HNT-EST beads are shown in Fig. 4b.

Similarly and as reported in the previous section, the bionanocomposite containing esterase immobilized on the CTS-HNT-EST presented the highest value of degradation, but no complete removal of DEHP was achieved (≈11 mg/L DEHP). The bionanocomposite of esterase immobilized on the ALG-HNT-EST was not able to completely degrade DEHP reaching a concentration of around 40 mg/L. It suggests that the availability of the immobilized enzyme for the degradation of the PAEs and their complexity are key factors in the degradation process. The analysis of the morphology of the bionanocomposites by SEM images (see supplementary material) could explain some of the causes of the different behavior being related to the distribution of HNT-EST in the composite. These images showed a higher availability of HNT containing enzyme on the surface of the CTS bionanocomposite in comparison with alginate and with a higher surface. Thus, when the volumetric flow was decreased and thus the residence time increased, DEHP concentration was found to be zero in the presence of CTS-HNT-EST bionanocomposite. The steady state was reached in all evaluated volumetric flows. Thus, the DEHP concentration was 27.64 mg/L for the column filled with ALG-HNT-EST bionanocomposite at 0.030 mL/min, while the value decreased to 23.6 mg/L when a lower volumetric flow was chosen (0.015 mL/min). As well as the reduction of the compound, the relative activity during the treatment process is an important factor to consider (Fig. 5b). At the end of the operation in continuous, CTS-HNT-EST bionanocomposite retained 81% of its initial activity, while ALG-HNT-EST bionanocomposite was able to maintain approximately 75% of its initial activity (Fig. 5b). Moreover, the enzyme mass (%) on CTS-HNT and ALG-HNT was found to be 85.48% and 79.2%, respectively. This may be because an amino group of CTS that is unreacted with GTA in the immobilization with the crosslinking method can adsorb PAEs and their metabolites (Dulazi and Liu 2011).

In addition, although CTS-HNT beads did not break or deform, ALG-HNT beads showed deformations upon completion of the experiment. This may be related to alginate having fast swelling behavior. Throughout the experiment, the solution with PAEs diffuses into the beads, thereby increasing the osmotic pressure inside the beads. The ALG-HNT beads may swell increasing their size, and eventually, the bead may collapse (Roquero et al., 2022). This may be the reason why ALG-HNT with esterase exhibits less degradation efficiency when compared to CTS-HNT with esterase.

4. Conclusions

Bionanocomposite beads based on esterase enzyme immobilized in halloysite nanotubes and natural polymers (chitosan and alginate) were successfully prepared and proved an improvement of the catalytic activity and other properties of the enzyme. The results demonstrated that they maintained their activity for a long period and the enzymatic degradability of PAEs is affected by the length of the alkyl side chain in their structures. CTS-HNT-EST are more effective and robust support material for the degradation of the pollutants in batch and continuous treatment. Both of them may act as strong candidates for the remediation of PAEs.

CRediT authorship contribution statement

Esin Balci: Investigation, Writing – original draft, Methodology, Formal analysis, Data curation. **Emilio Rosales:** Investigation, Methodology, Validation, Formal analysis, Writing – review & editing. **Marta Pazos:** Funding acquisition, Supervision, Writing – review & editing. **Aysun Sofuoglu:** Writing – review & editing. **Maria Angeles Sanroman:** Supervision, Funding acquisition, Project administration, Conceptualization, Writing – review & editing.

Declaration of Competing Interest

The authors declare that they have no known competing financial interests. As Maria Angeles Sanroman, a [co-]author on this paper, is the associate editor of Bioresource Technology, she was blinded to this paper during review, and the paper was independently handled by Samir Kumar Khanal as editor.

Data availability

Data will be made available on request.

Acknowledgments

This research was funded through the join 2019-2020 Biodiversa & Water JPI joint call for research proposals, under the BiodivRestore ERA-Net COFUND programme. Project PCI2022-132941 funded by MCIN/AEI /10.13039/501100011033 and European Union Next Generation EU/PRTR and Xunta de Galicia and ERDF (ED431C 2021-43). Additionally, the research has been provided with the financial support by the Scientific and Technological Research Council of Turkey (TUBITAK) under 2214-A Doctoral Research Fellowship Program. Funding for open access charge: Universidade de Vigo/CISUG.

Appendix A. Supplementary data

Supplementary data to this article can be found online at https://doi.org/10.1016/j.biortech.2022.127990.

References

Ahn, J.Y., Kim, Y.H., Min, J., Lee, J., 2006. Accelerated degradation of dipentyl phthalate by *Fusarium oxysporum f. sp.* pisi cutinase and toxicity evaluation of its degradation products using bioluminescent bacteria. Curr. Microbiol. 52, 340–344. https://doi.org/10.1007/s00284-005-0124-9.

Ahuactzin-Perez, M., Tlecuitl-Beristain, S., Garcia-Davila, J., Santacruz-Juarez, E., Gonzalez-Perez, M., Gutierrez-Ruiz, M.C., Sanchez, C., 2018. Kinetics and pathway of biodegradation of dibutyl phthalate by *Pleurotus ostreatus*. Fungal Biol. 122, 991–997. https://doi.org/10.1016/j.funbio.2018.07.001.

Bhagyaraj, S., Krupa, I., 2020. Alginate-halloysite nanocomposite aerogel: preparation, structure, and oil/water separation applications. Biomolecules 10, 1632. https://doi.org/10.3390/biom10121632.

Bradford, M.M., 1976. A rapid and sensitive method for the quantitation of microgram quantities of protein utilizing the principle of protein-dye binding. Anal. Biochem. 72 (1-2), 248–254.

Chen, J.P., Lin, Y.S., 2007. Decolorization of azo dye by immobilized *Pseudomonas luteola* entrapped in alginate-silicate sol-gel beads. Process Biochem. 42, 934–942. https://doi.org/10.1016/j.procbio.2007.03.001.

Choo, C.K., Kong, X.Y., Goh, T.L., Ngoh, G.C., Horri, B.A., Salamatinia, B., 2016. Chitosan/Halloysite beads fabricated by ultrasonic-assisted extrusion-dripping and a case study application for copper ion removal. Carbohydr. Polym. 138, 16–26. https://doi.org/10.1016/j.carbpol.2015.11.060.

Clark, K., Cousins, I.T., MacKay, D., Yamada, K., 2003. Observed concentrations in the environment. In: Staples, C.A. (Ed.), Handbook of Environmental Chemistry. Springer, Berlin, Heidelberg, pp. 125–177. https://doi.org/10.1007/b11465.

Das, M.T., Ghosh, P., Thakur, I.S., 2014. Intake estimates of phthalate esters for the South Delhi population based on exposure media assessment. Environ. Pollut. 189, 118–125. https://doi.org/10.1016/j.envpol.2014.02.021.

Ding, J., Wang, C., Xie, Z., Li, J., Yang, Y., Mu, Y., Tang, X., Xu, B.o., Zhou, J., Huang, Z., Lei, B., 2015. Properties of a newly identified esterase from *Bacillus sp.* K91 and its novel function in diisobutyl phthalate degradation. PLoS ONE 10 (3), e0119216.

Duce, C., Bramanti, E., Ghezzi, L., Bernazzani, L., Bonaduece, I., Colombini, M.P., Spepi, A., Biagi, S., Tine, M.R., 2013. Interactions between inorganic pigments and proteinaceous binders in reference paint reconstructions. Dalton Trans. 42, 5975–5984. https://doi.org/10.1039/C2DT32203J.

Duce, C., Porta, V.D., Bramanti, E., Campanella, B., Spepi, A., Tine, M.R., 2017. Loading of halloysite nanotubes with BSA, α-Lac, and β-Lg: a fourier transform infrared spectroscopic and thermogravimetric study. Nanotechnology 28 (5), 055706. https://doi.org/10.1088/1361-6528/28/5/055706.

Dulazi, A.A., Liu, H., 2011. Removal of phthalate esters from water using immobilized lipase on chitosan beads. Environ. Technol. 32 (13), 1443–1451. https://doi.org/10.1080/09593330.2010.538932.

Fang, Y., Zhang, L., Wang, J., Zhou, Y., Bangce, Y.E., 2017. Biodegradation of phthalate esters by a newly isolated *Acinetobacter sp.* strain LMB-5 and characteristics of its esterase. Pedosphere 27 (3), 606–615. https://doi.org/10.1016/S1002-0160(17)60355-2.

Feng, Z., Kunyan, C., Jiamo, F., Guoying, S., Huifang, Y., 2002. Biodegradability of di(2-ethylhexyl) phthalate by *Pseudomonas fluorescens* FS1. Water, Air, Soil Pollut. 140, 297–305. https://doi.org/10.1023/A:1020108502776.

Fitter, J., Hermann, R., Dencher, N.A., Blume, A., Hauss, T., 2001. Activity and stability of a thermostable α-amylase compared to its mesophilic homologue: mechanism of thermal adaptation. Biochemistry 40 (35), 10723–10731. https://doi.org/10.1021/bi010808b.

Gao, M., Dong, Y., Zhang, Z.e., Song, Z., 2020. Effect of dibutyl phthalate on microbial function diversity and enzyme activity in wheat rhizosphere and non-rhizosphere soils. Environ. Poll. 265, 114800.

Handayani, N., Loss, K., Wahyuningrum, D., Zulfikar, M.A., 2012. Immobilization of Mucor miehei lipase onto macroporous polyethersulfone membrane for enzymatic reactions. Membranes 2, 198–213. https://doi.org/10.3390/membranes2020198.

He, H., Zhang, S., Liu, X., 2015. Immobilization of feruloyl esterases on magnetic nanoparticles and its potential in production of ferulic acid. J. Biosci. Bioeng. 120 (3), 330–334. https://doi.org/10.1016/j.jbiosc.2015.01.006.

Hung, T.C., Giridhar, R., Chiou, S.H., Wu, W.T., 2003. Binary immobilization of *Candida rugose* lipase on chitosanü. J. Mol. Catal. B Enzym. 26, 69–78. https://doi.org/10.1016/S1381-1177(03)00167-X.

Hurmuzlu, R., Okur, M., Saracoglu, N., 2021. Immobilization of Trametes versicolor laccase on chitosan/halloysite as a biocatalyst in the removal RR dye. Int. J. Biol. Macromol. 192, 331–341. https://doi.org/10.1016/j.ijbiomac.2021.09.213.

Jang, H., Yang, S., Kong, J., Dong, A., Yu, S., 2015. Obtaining information about protein secondary structures in aqueous solution using Fourier transform IR spectroscopy. Nat. Protoc. 10 (3), 382–396. https://doi.org/10.1038/nprot.2015.024.

Kim, Y.H., Lee, J., 2005. Enzymatic degradation of dibutyl phthalate and toxicity of its degradation products. Biotechnol. Lett. 27, 635–639. https://doi.org/10.1007/s10529-005-3631-7.

Kumar, V., Sharma, N., Maitra, S.S., 2017. Comparative study on the degradation of dibutyl phthalate by two newly isolated *Pseudomonas sp. V21b* and *Comamonas sp. 51F*. Biotechnol. Reports 15, 1–10. https://doi.org/10.1016/j.btre.2017.04.002.

Liang, D.W., Zhang, T., Fang, H.H.P., He, J., 2008. Phthalates biodegradation in the environment. Appl. Microbiol. Biotechnol. 80, 183–198. https://doi.org/10.1007/s00253-008-1548-5.

Lisuzzo, L., Cavallaro, G., Milioto, S., Lazzara, G., 2020. Halloysite nanotubes coated by chitosan for the controlled release of khellin. Polymers. 12, 1766. https://doi.org/10.3390/polym12081766.

Luo, P., Zhao, Y., Zhang, B., Liu, J., Yang, Y., Liu, J., 2010. Study on the adsorption of Neutral Red from aqueous solution onto halloysite nanotubes. Water Res. 44, 1489–1497. https://doi.org/10.1016/j.watres.2009.10.042.

Mondal, S., Li, C., Wang, K., 2015. Bovine serum albumin adsorption on glutaraldehyde cross-linked chitosan hydrogels. J. Chem. Eng. Data 60, 2356–2362. https://doi.org/10.1021/acs.jced.5b00264.

Niazi, J.H., Prasad, D.T., Karegoudar, T.B., 2001. Initial degradation of dimethylphthalate by esterases from Bacillus species. FEMS Microbiol. Lett. 196 (2), 201–205. https://doi.org/10.1111/j.1574-6968.2001.tb10565.x.

Okamoto, Y., Toda, C., Ueda, K., Hashizume, K., Kojima, N., 2011. Transesterification in the microbial degradation of phthalate esters. J. Health Sci. 57 (3), 293–299. https://doi.org/10.1248/jhs.57.293.

Olshansky, Y., Masaphy, S., Root, R.A., Rytwo, G., 2018. Immobilization of *Rhus vernicifera* laccase on sepiolite; effect of chitosan and copper modification on laccase adsorption and activity. Appl. Clay Sci. 152, 143–147. https://doi.org/10.1016/j.clay.2017.11.006.

Peng, Q., Liu, M., Zheng, J., Zhou, C., 2015. Adsorption of dyes in aquesous solutions by chitosan-halloysite nanotubes composite hydrogel beads. Micropor. Mesopor. Mat. 201, 190–201. https://doi.org/10.1016/j.micromeso.2014.09.003.

Ramsay, J.A., Mok, W.H.W., Luu, Y.S., Savage, M., 2005. Decoloration of textile dyes by alginate-immobilized *Trametes versicolor*. Chemosphere 61 (7), 956–964. https://doi.org/10.1016/j.chemosphere.2005.03.070.

Ren, L., Jia, Y., Ruth, N., Qiao, C., Wang, J., Zhap, B., Yan, Y., 2016. Biodegradation of phthalic acid esters by a newly isolated *Mycobacterium sp*. YC-RL4 and the bioprocess with environmental samples. Environ. Sci. Pollut. Res. 23, 16609–16619. https://doi.org/10.1007/s11356-016-6829-4.

Roquero, D.M., Othman, A., Melman, A., Katz, E., 2022. Iron (III)-croslinked alginate hydrogels: a critical review. Mat. Adv. 3, 1849–1873. https://doi.org/10.1039/d1ma00959a/.

Saito, T., Tanabe, R., Nagai, K., Kato, K., 2010. Enzymatic hydrolysis of structurally diverse phthalic acid esters by porcine and bovine pancreatic cholestral esterases. Chemosphere 81, 1544–1548. https://doi.org/10.1016/j.chemosphere.2010.08.020.

Singh, N., Dalal, V., Mahto, J.K., Kumar, P., 2017. Biodegradation of phthalic acid esters (PAEs) and in silico structural characterization of mono-2-ethylhexyl phthalate (MEHP) hydrolase on the basis of close structural homolog. J. Hazard. Mater. 338, 11–22. https://doi.org/10.1016/j.jhazmat.2017.04.055.

Staples, C.A., Peterson, D.R., Parkerton, T.F., Adams, W.J., 1997. The environmental fate of phthalate esters: A literature review. Chemosphere 35 (4), 667–749. https://doi.org/10.1016/S0045-6535(97)00195-1.

Sun, J., Zhu, H., Yang, X., Zheng, Y., Sun, T., Xu, H., Meng, J., Zhang, A., 2022. Carboxylesterase and lipase-catalyzed degradation of phthalate esters in soil and water: Congener structure selectivity and specificity. Environ. Technol. Innovation 28, 102571. https://doi.org/10.1016/j.eti.2022.102571.

Tekedar, H.C., Sanli-Mohamed, G., 2011. Molecular cloning, over expression, and characterization of thermoalkalophilic esterases isolated from *Geobasillus sp*. Extremophiles 15, 203–211. https://doi.org/10.1007/s00792-010-0344-1.

Tercan, Ç., Sürmeli, Y., Şanlı-Mohamed, G., 2021. Thermoalkalophilic recombinant esterase entrapment in chitosan/calcium/alginate-blended beads and its characterization. J. Chem. Technol. Biotechnol. 96, 2257–2264. https://doi.org/10.1002/jctb.6750.

Wang, Y.P., Gu, J.D., 2006. Degradation of Dimethyl Isophthalate by Viarovorax paradoxus Strain T4 Isolated from Deep-Ocean sediment of the South China sea. Hum. Ecol. Risk. Assess. Int. J. 12, 236–247. https://doi.org/10.1080/10807030500531521.

Wang, Y., Li, F., Ruan, X., Song, J., Lv, L.v., Chai, L., Yang, Z., Luo, L., Franzetti, A., 2017. Biodegradation of di-n-butyl phthalate by bacterial consortium LV-1 enriched from river sludge. PLoS ONE 12 (5), e0178213.

Wei, L., Wang, S., Zhang, F., Fan, Y., Liao, Y., Liao, B., Wang, W., Tu, J., Xiao, J., Wu, G., Zhang, Z., 2022. Efficient degradation of molasses wastewater from sugar mill by lipase via addition. LWT Food Sci. Technol. 161, 113366 https://doi.org/10.1016/j.lwt.2022.113366.

Weizhen, Z., Xiaowei, Z., Peng, G.u., Ning, W., Zini, L., Jian, H.e., Zheng, Z., 2020. Distribution and risk assessment of phthalates in water and sediment of the Pearl River Delta. Environ. Sci. Pollut. Res. 27 (11), 12550–12565.

Yang, T., Ren, L., Jia, Y., Fan, S., Wang, J., Wang, J., Nahurira, R., Wang, H., Yan, Y., 2018. Biodegradation of di (2-ethylhexyl) phthalate by *Rhodococcus ruber* YC-YT1 in contaminated water and soil. Int. J. Environ. Res. Public Health 15, 964. https://doi.org/10.3390/ijerph15050964.

Yoo, W., Kim, B., Jeon, S., Kim, K.K., Kim, T.D., 2020. Identification, characterization, and immobilization of a novel YbfF esterase from *Halomonas elongata*. Int. J. Biol. Macromol. 165, 1139–1148. https://doi.org/10.1016/j.ijbiomac.2020.09.247.

Zhai, R., Zhang, B., Wan, Y., Li, C., Wang, J., Liu, J., 2013. Chitosan-halloysite hybrid nanotubes: horseradish peroxidase immobilization and applications in phenol removal. Chem. Eng. J. 214, 304–309. https://doi.org/10.1016/j.cej.2012.10.073.

Zhang, X.Y., Fan, X., Qiu, Y.J., Li, C.Y., Xing, S., Zheng, Y.T., Xu, J.H., 2014. Newly identified thermostable esterase from *Sulfobacillus acidophilus*: properties and performance in phthalate ester degradation. Appl. Environ. Microbiol. 80 (22), 6870–6878. https://doi.org/10.1128/AEM.02072-14.